



Microstructure and mechanical properties of aluminum matrix composites produced by Al-La₂O₃ in-situ reaction

C. Zhou^{a,b,1}, M. Lv^{a,b,1}, Y.N. Zan^{a,c,*}, Y. Liu^{a,b}, X.H. Shao^a, Q.Z. Wang^{a,c}, D. Wang^a, B.L. Xiao^a, Z.Y. Ma^{a,c}

^a Shi-changxu Innovation Center for Advanced Materials, Institute of Metal Research, Chinese Academy of Sciences, 72 Wenhua Road, Shenyang 110016, China

^b School of Materials Science and Engineering, University of Science and Technology of China, 72 Wenhua Road, Shenyang 110016, China

^c Key Laboratory of Nuclear Materials and Safety Assessment, Institute of Metal Research, Chinese Academy of Sciences, 72 Wenhua Road, Shenyang 110016, China

ARTICLE INFO

Keywords:

Aluminum matrix composites
High energy ball milling
Microstructure
Mechanical properties

ABSTRACT

In this study, composites reinforced by amorphous Al₂O₃ (am-Al₂O₃) and Al₁₁La₃ particles, formed through Al-La₂O₃ in-situ reaction, were fabricated by high energy ball milling (HEBM) and hot-pressing. The difference in high-temperature strength of composites hot-pressed at different temperatures could be as high as 44%, and the reason was disclosed by careful microstructure characterization. It was found that the in-situ reaction could be divided into three processes, accompanied by the crystallization of am-Al₂O₃ and coarsening of Al₁₁La₃. Am-Al₂O₃ could not only directly strengthen the composites, but also inhibit the coarsening of Al₁₁La₃ by forming a film on its surface. Therefore, when the hot-pressing temperature reached the crystallization temperature of am-Al₂O₃ (590 °C), am-Al₂O₃ film transformed into discontinuous γ-Al₂O₃ particles, resulting in rapid coarsening of Al₁₁La₃ as well as the degeneration of strengthening efficiency. By maintaining Al₂O₃ in an amorphous state and Al₁₁La₃ in fine size, the highest tensile strength of the composites could reach 190 MPa at 350 °C.

1. Introduction

Due to excellent mechanical properties such as high specific strength and specific modulus, Al alloys have become important lightweight materials and are widely used in aerospace, nuclear industry, and automotive fields as load-bearing components [1–3]. As equipment in these fields develops to new generations, higher requirements for high-temperature properties of materials have been put forward, especially for long-term thermostability. In many applications, steel and titanium alloys are irreplaceably used, which greatly restricts the lightweight of equipment.

Therefore, heat-resistant Al alloys are desired to be competent structural materials at higher temperatures, especially at 300–400 °C, which could avoid excessive application of high-density materials. Under this demand, heat-resistant Al alloys have appeared [4–6]. However, metastable precipitates in Al alloys would quickly coarsen at high temperatures, decreasing the high-temperature strength of Al alloys significantly [7]. Even Al alloys designed for high-temperature

applications such as Al-Si-Cu and Al-Cu alloys could hardly serve at above 300 °C for long-term application.

Aluminum matrix composites (AMCs) reinforced by ceramic particles could exhibit reliable thermostability because of the stable reinforcements. However, traditional micro-sized reinforcements only provide limited strengthening effects for high-temperature strength [6,8]. Nano-sized reinforcements could be effective in enhancing high-temperature strength, but their content in AMCs is usually limited, so the strengthening efficiency is crucial to realize high strength.

It was found that nano-sized in-situ amorphous Al₂O₃ (am-Al₂O₃) film formed on the surfaces of Al powders could not only be highly effective in enhancing the high-temperature strength of Al₂O₃/Al [8–11] but also be deformable during the tensile process, which is expected to exert fewer detrimental effects on the ductility of AMCs [12]. Am-Al₂O₃ also possesses the ability to be stable until the temperature reaches its crystallization temperature, which was reported to be over 550 °C [13].

However, the content of the native am-Al₂O₃ is limited by the size and specific surface area of Al powders. Increasing the content of am-

* Corresponding author at: Shi-changxu Innovation Center for Advanced Materials, Institute of Metal Research, Chinese Academy of Sciences, 72 Wenhua Road, Shenyang 110016, China.

E-mail address: ynzan15b@imr.ac.cn (Y.N. Zan).

¹ These authors contributed equally to this work.

<https://doi.org/10.1016/j.matchar.2022.111887>

Received 25 February 2022; Accepted 4 April 2022

Available online 9 April 2022

1044-5803/© 2022 Elsevier Inc. All rights reserved.

Al_2O_3 requires the use of finer Al powders, which is accompanied by higher costs and preparation risks. It should be noticed that in-situ Al_2O_3 could also be formed via reaction between Al and some metal oxides such as CuO , ZrO_2 , TiO_2 , etc. [14–16]. However, these in-situ reactions could only be thermally activated and occur during the sintering process at temperatures higher than the crystallization temperature of am- Al_2O_3 , generating $\gamma\text{-Al}_2\text{O}_3$, which had low efficiency in strengthening [17]. Therefore, it is valuable to look for efficient and controllable ways to introduce in-situ am- Al_2O_3 into the Al matrix at temperatures lower than the crystallization temperature of am- Al_2O_3 .

It has been found that the intense mechanical effect in high energy ball milling (HEBM) can decrease in-situ reaction temperature, and even stimulate reaction during the milling process [18]. From this aspect, it is expected that the in-situ reaction can be stimulated at room temperature by the HEBM process and produce am- Al_2O_3 . So, it is worth trying to fabricate in-situ am- Al_2O_3 reinforced AMCs with excellent high-temperature strength by choosing a suitable in-situ reaction system via HEBM [19–21].

Adding rare earth elements such as La, Ce, and Er into Al alloys could produce desirable positive effects on high-temperature properties by forming thermostable intermetallic compounds [22–26]. Sakamoto et al. [27] reported that the formation of intermetallic compound $\text{Al}_{11}\text{La}_3$ from the Al- La_2O_3 reaction was much easier thanks to the high binding energy of Al-La. However, in Sakamoto et al.'s study, constrained by the energy input of the ball milling, Al_2O_3 was formed in the sintering process rather than the HEBM process and identified to be $\gamma\text{-Al}_2\text{O}_3$, which had a lower strengthening effect than am- Al_2O_3 [17].

Herein, HEBM of Al- La_2O_3 was put forward as a promising way to generate in-situ am- Al_2O_3 , forming (am- Al_2O_3 + $\text{Al}_{11}\text{La}_3$)/Al for the first time. The aims of this study are (a) to verify the possibility of producing in-situ am- Al_2O_3 by HEBM, (b) to elucidate the evolution of reinforcing phases in the hot-pressing process, and (c) to identify the relationship between microstructure and mechanical properties of the composites.

2. Experimental

Pure Al powders and La_2O_3 particles with mean sizes of 13 μm and 300 nm, respectively, as shown in Fig. 1, were utilized in the fabrication of the composites. 8 wt% La_2O_3 particles and Al powders were ball milled using an attritor with a ball-to-powder ratio of 15:1 at 400 rpm for 6 h in an argon atmosphere. 2 wt% stearic acid was used as the process control agent.

The mixed powders after HEBM were vacuum degassed at 400 °C and then hot-pressed at 510 °C, 530 °C, 550 °C, 570 °C, 590 °C, and 610 °C, respectively, for 2 h under the vacuum of about 10^{-1} Pa, nominated as HP 510, HP 530, HP 550, HP 570, HP 590, and HP 610, respectively. Finally, the billets were all extruded at 450 °C into bars with an

extrusion ratio of 16:1.

The phases in the composites were investigated by X-ray diffraction (XRD). The microstructure of the composites was observed using scanning electron microscopy (SEM, FEI Inspect F50) and transmission electron microscopy (TEM, FEI Talos F200X G2). Specimens for SEM observation were ground with 5000 grit abrasive paper and then mechanically polished using SiO_2 polishing liquid. Specimens for TEM observation were prepared by metallographic grinding and dimpling, followed by ion-milling using a Gatan PIPS (Model 695).

Dog-bone tensile specimens with a gauge length of 15 mm, a width of 4 mm, and a thickness of 2 mm were machined parallel to the extrusion direction. The tensile test was carried out at room temperature and 350 °C using Instron 8801 tester and MTS E45. 105 tester. A strain rate of $1 \times 10^{-3} \text{ s}^{-1}$ was used. At least 3 specimens were tested for each sample.

3. Results

3.1. Microstructure of the composites

The SEM micrographs of Al- La_2O_3 mixed powders after HEBM are shown in Fig. 2. It could be seen that after 6 h of HEBM, fine particles were evenly dispersed in the Al powders.

The XRD pattern of the Al- La_2O_3 mixed powders after HEBM is shown in Fig. 3. Besides the peaks of Al and La_2O_3 , $\text{Al}_{11}\text{La}_3$ diffraction peaks were evidently observed, proving that the in-situ reaction between Al and La_2O_3 happened in the HEBM process.

Fig. 4 shows the XRD patterns of the composites hot-pressed at different temperatures. The peaks of La_2O_3 and $\text{Al}_{11}\text{La}_3$ were seen in all composites. XRD patterns of HP 510 and HP 530 exhibited the same characteristics. When the hot-pressing temperature increased to 550 °C and higher, more peaks of $\text{Al}_{11}\text{La}_3$ appeared gradually with their intensity increasing, especially when the hot-pressing temperature reached 590 °C and 610 °C. The peaks of La_2O_3 exhibited the opposite tendency, and the significant change also occurred at 590 °C and 610 °C. It indicated that Al and La_2O_3 reacted gradually with the increase of hot-pressing temperature in the temperature range of 530–590 °C, and the reaction became more complete in the temperature range of 590–610 °C.

Fig. 5 displays the SEM micrographs of the composites with different hot-pressing temperatures. By Energy Dispersion Spectrum (EDS) analysis, two kinds of particles were identified. One particle of each kind is indicated by A and B in Fig. 5c representatively. Table 1 presents the EDS results of Spots A and B. The A-phases contained O and La elements, indicating that the A-phases were unreacted La_2O_3 . The B-phases consisted of Al and La elements, indicating that the B-phases were $\text{Al}_{11}\text{La}_3$. In these low-magnification SEM images, no evident difference was

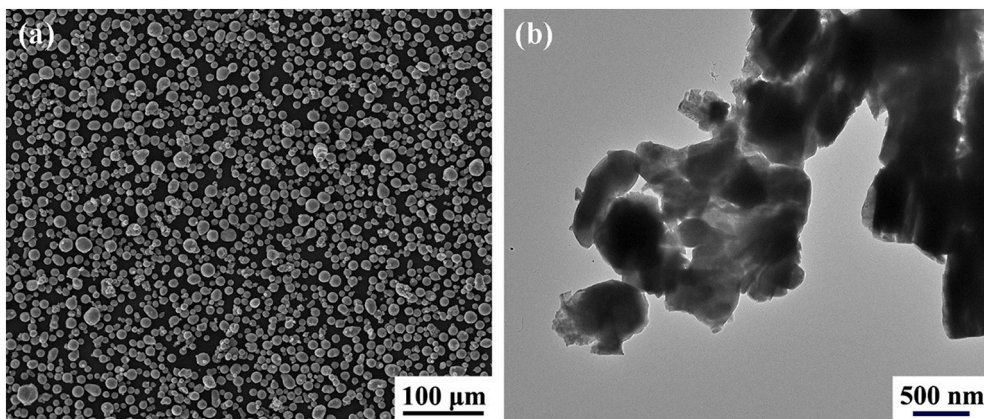


Fig. 1. Morphologies of (a) pure Al powders and (b) La_2O_3 particles.

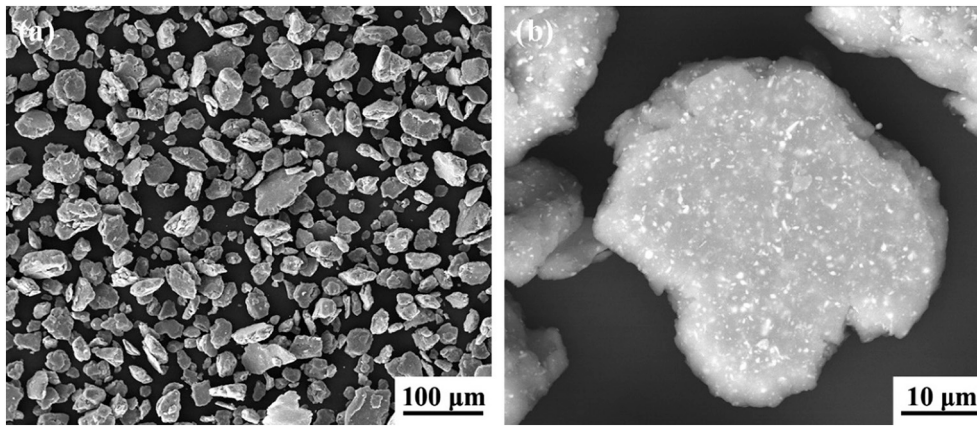


Fig. 2. SEM images of Al-La₂O₃ mixed powders after HEBM with (a) low and (b) high magnifications.

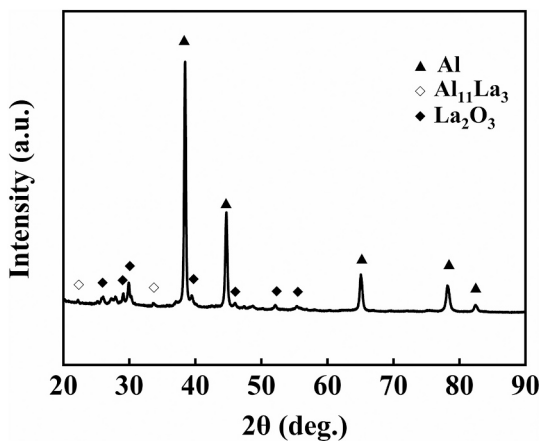


Fig. 3. XRD pattern of the Al-La₂O₃ mixed powders after HEBM.

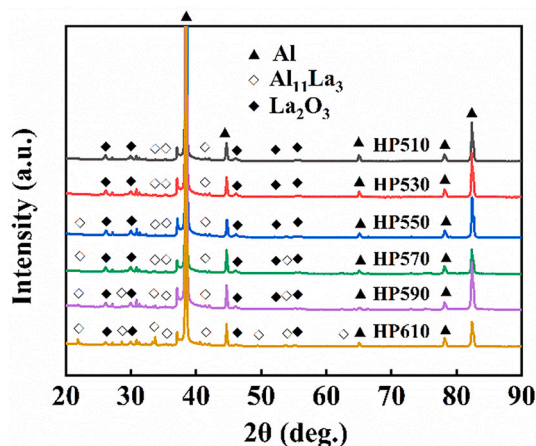


Fig. 4. XRD patterns of the composites with different hot-pressing temperatures.

revealed in HP 510, HP 530, HP 550, and HP 570. With the hot-pressing temperature increasing to 590 °C, more and larger Al₁₁La₃ were observed obviously (denoted by red arrows), which was consistent with the XRD results. When the temperature increased to 610 °C, Al₁₁La₃ phases grew to much larger scales (about 1–2 μm in diameter). In these images, Al₂O₃ cannot be detected due to its small size.

TEM images of HP 510, HP 550, and HP 610 are shown

representatively in Fig. 6 to reveal the microstructure evolution under the effect of hot-pressing temperature. It was shown that the size of the particles increased with the increase of hot-pressing temperature, while the quantity decreased. When the temperature increased to 610 °C, particles increased to a few microns, which was in accord with SEM images.

Figs. 7a and b show the STEM-BF images of HP 510 and HP 550. Compared with the TEM images shown in Fig. 6, the contrast of the STEM-BF images was more sensitive to the elemental composition. Two kinds of phases exhibiting black and gray contrasts were disclosed in Fig. 7a and b. By EDS analysis and elemental mapping shown in Fig. 7c, it was found that the black phases in Fig. 7a contained a high content of La and O elements, while Al element was absent in these phases. So, these particles could be presumed to be unreacted La₂O₃ particles. Gray phases were found to contain a certain amount of Al and La elements, so they were identified to be Al₁₁La₃, which could further be confirmed by high-resolution TEM (HRTEM) image, as shown in Fig. 7d. Besides Al and La elements, a small amount of O element was found in Al₁₁La₃, which would be discussed in the following part. Furthermore, Al₁₁La₃ exhibited bimodality in size distribution. Besides particles with a size of over 200 nm, many particles with a size of about 30 nm could also be observed. By comparing Fig. 7a and b, it could be concluded that Al₁₁La₃ became coarser under higher hot-pressing temperatures. Larger Al₁₁La₃ with a size of over even 500 nm were formed.

More microstructural details of HP 550 are shown in Fig. 8a with higher magnification. The STEM-BF and elemental mapping images in square A are shown in Fig. 8b and c, and the elemental mapping image in square B is shown in Fig. 8d. It was found that these fine Al₁₁La₃ and La₂O₃ particles were commonly surrounded by oxygenated chemicals, which could explain the small amount of O element in Al₁₁La₃. Since no other element concentration was revealed, it could be speculated that these particles are am-Al₂O₃ formed in the in-situ reaction, which could be confirmed by the HRTEM image shown in Fig. 8e. The semi-transparent state shown in the TEM image was also in accord with am-Al₂O₃ in the previous study [28]. It could be concluded that the am-Al₂O₃ around the Al₁₁La₃ phases could effectively inhibit the coarsening of the Al₁₁La₃. In addition to being distributed around fine Al₁₁La₃ and La₂O₃ particles, am-Al₂O₃ was also found to disperse in the Al matrix (red circles).

The microstructure of HP 610 is shown in Fig. 9. When the hot-pressing temperature increased to 610 °C, although the reaction between La₂O₃ and Al matrix became more complete, there were still a few unreacted La₂O₃ particles left (phase A denoted by yellow arrows). Nano-sized particles (including La₂O₃ and Al₁₁La₃) became much fewer and micro-sized Al₁₁La₃ particles (phase B) were formed. By observing Fig. 9d and e, many fine particles containing O but not La element were found, indicating nano-sized Al₂O₃ particles were dispersed in the Al

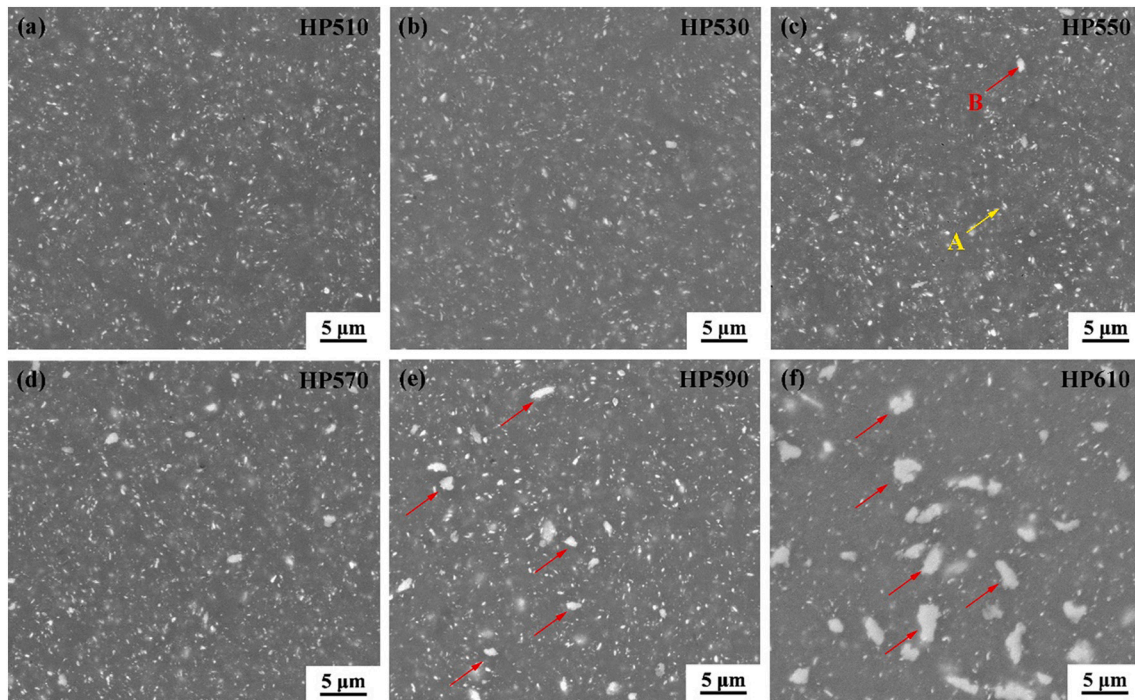


Fig. 5. SEM images of (a) HP 510, (b) HP 530, (c) HP 550, (d) HP 570, (e) HP 590 and (f) HP 610.

Table 1
EDS results of Spot A and Spot B.

Element	Al		La		O	
	Wt%	At.%	Wt%	At.%	Wt%	At.%
Spot A	77.04	82.50	14.99	3.12	7.96	14.38
Spot B	57.82	87.59	42.18	12.41	0	0

matrix.

In the STEM image of HP 610 with higher magnification (Fig. 10a) and its corresponding EDS mapping (Fig. 10b), Al_2O_3 particles were revealed to exhibit an acicular morphology, which was different from am- Al_2O_3 in HP 510 or HP 550 as shown in Fig. 8. It was identified to be $\gamma\text{-Al}_2\text{O}_3$ by HRTEM (Fig. 10c).

It should be noted that there is a critical temperature, above which am- Al_2O_3 will transform into $\gamma\text{-Al}_2\text{O}_3$, as reported in previous studies [28]. The crystallization temperature of am- Al_2O_3 is usually discrepant in different studies and is believed to be influenced by its own morphology and defects [6,28,29]. By observing TEM images of HP 570 and HP 590 shown in Fig. 11, it was found that only am- Al_2O_3 (denoted by red arrows, around other phases or in Al matrix) was present in HP 570, and $\gamma\text{-Al}_2\text{O}_3$ (denoted by blue arrows, in Al matrix) with the acicular morphology started to appear in HP 590. Therefore, it could be

concluded that in this study, am- Al_2O_3 started to transform into $\gamma\text{-Al}_2\text{O}_3$ at 590 °C, and the transformation could be finished completely at 610 °C.

Furthermore, continuous am- Al_2O_3 film between Al matrix and fine particles (La_2O_3 and $\text{Al}_{11}\text{La}_3$) transformed into discontinuous $\gamma\text{-Al}_2\text{O}_3$ in HP 590 and HP 610, which meant that the barrier to Al- La_2O_3 reaction and growth of $\text{Al}_{11}\text{La}_3$ disappeared. Therefore, it could explain the temperature threshold of 590 °C for $\text{Al}_{11}\text{La}_3$ particles to grow up much more quickly in the composites.

3.2. Mechanical properties

The tensile stress-strain curves of the composites are shown in Fig. 12 and the mechanical properties are listed in Table 2. With the increase of hot-pressing temperature, the tensile properties of the composites decreased at both room temperature (RT) and 350 °C. The highest tensile strengths of 406 MPa at RT and 190 MPa at 350 °C were achieved when the hot-pressing temperature was 510 °C. The tensile strength at RT and 350 °C decreased to 327 MPa and 132 MPa, respectively, when the hot-pressing temperature was 610 °C. Elongation increased with the decrease of tensile strength.

It should be noted that when the hot-pressing temperature was over 570 °C (corresponding to the temperature at which reaction became more sufficient and $\text{Al}_{11}\text{La}_3$ coarsened quickly), the decreasing trend of

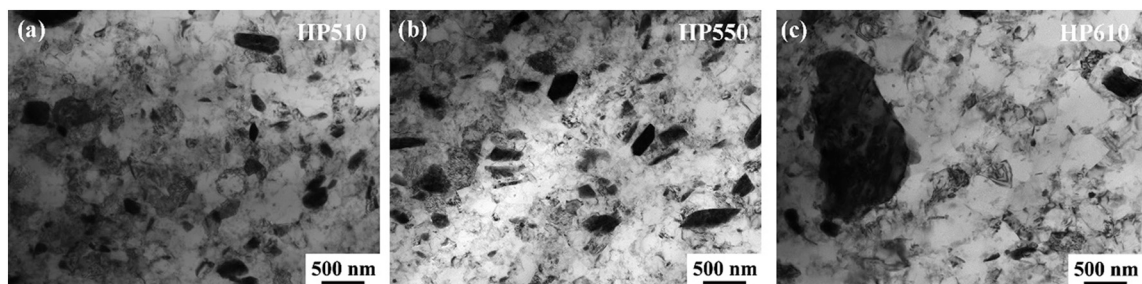


Fig. 6. TEM images of (a) HP 510, (b) HP 550, and (c) HP 610.

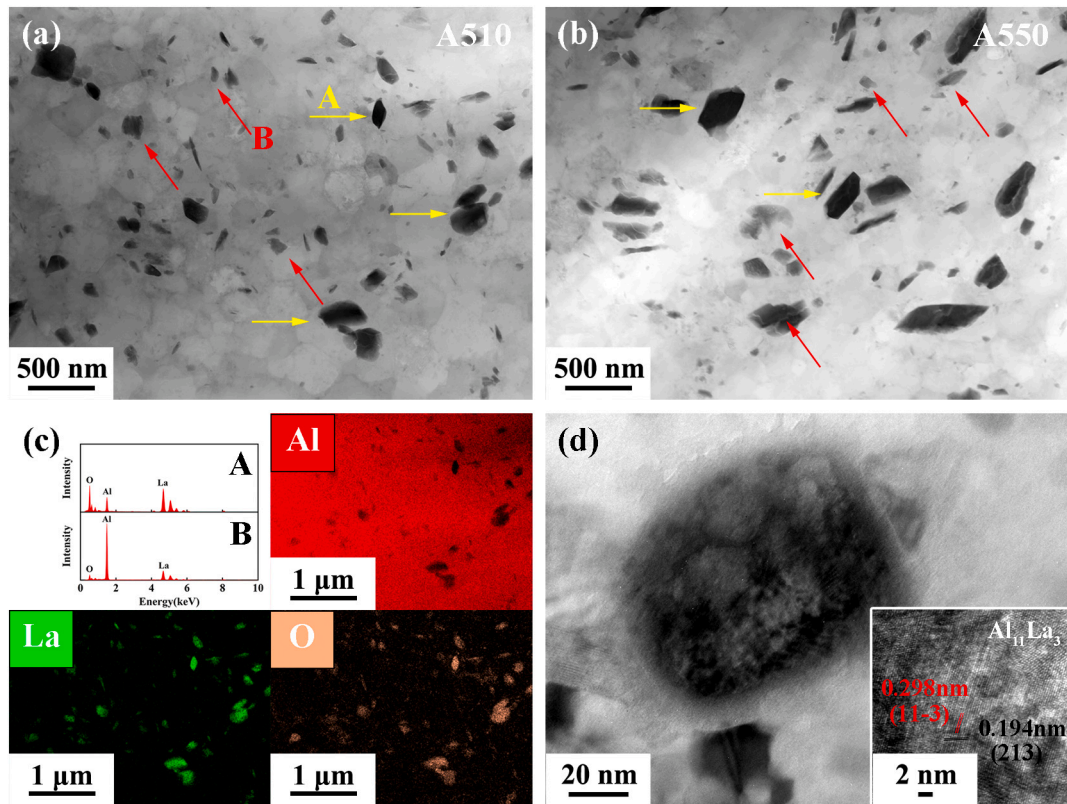


Fig. 7. STEM-BF images of (a) HP 510 and (b) HP 550, and (c) EDS results of the same position of (a), and (d) TEM image of an $\text{Al}_{11}\text{La}_3$ particle in HP 510 with its HRTEM image in the inset.

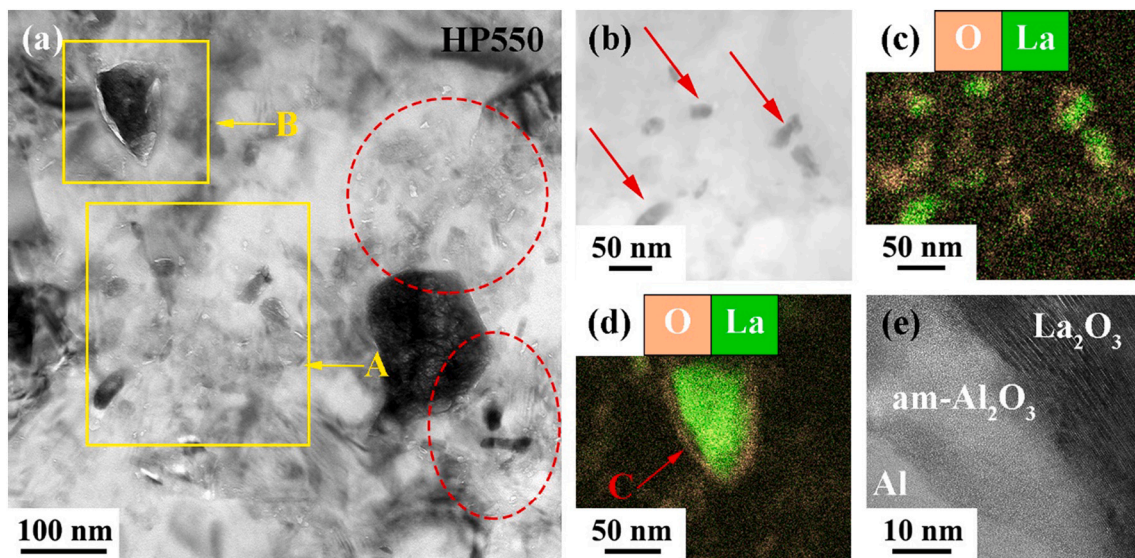


Fig. 8. (a) TEM image of HP 550, (b) STEM-BF image of position A, EDS mapping of positions (c) A and (d) B, and (e) magnified view of position C.

RT strength slowed down, but the high-temperature strength declined even more rapidly with the increase of hot-pressing temperature.

3.3. Fractographs

Fig. 13 displays the SEM fracture surfaces of HP 550 and HP 610 at RT and 350 °C. The RT fractographs (Fig. 13a and b) exhibited the characteristic of obvious dimples. In the fractograph of HP 610, lots of large $\text{Al}_{11}\text{La}_3$ particles were disclosed. Some cracks were also found in

large $\text{Al}_{11}\text{La}_3$ particles (inset in Fig. 13b), which were probably formed in the tensile process [30].

Unlike the fracture surfaces at RT, an intergranular fracture characteristic was observed at 350 °C, as shown in Fig. 13c and d. Fig. 13c exhibited a finer structure than Fig. 13d, which was in accord with finer grains in HP 550. Furthermore, in Fig. 13c and d, a mass of nano-sized particles could be observed on the fracture surfaces. Furthermore, compared to that in HP 610 (Fig. 13d), more particles were disclosed in HP 550 (Fig. 13c), being consistent with the higher content of nano-

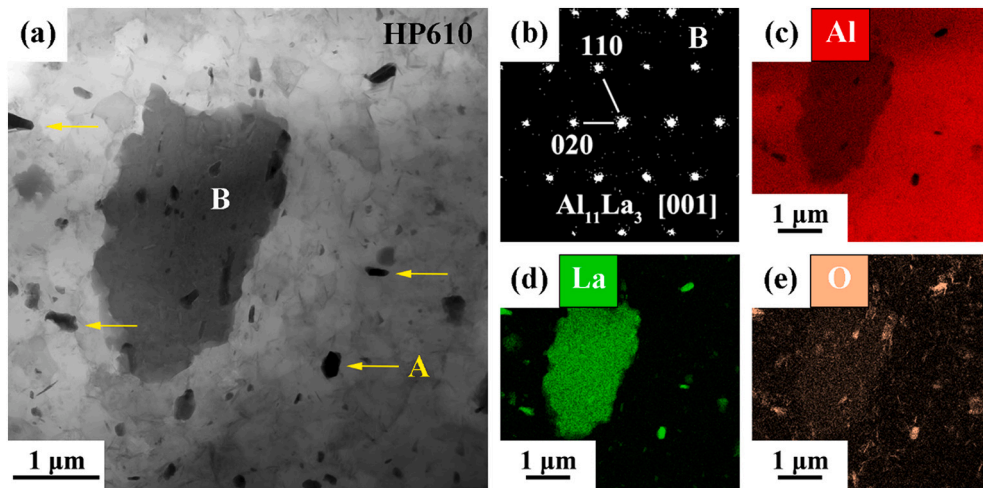


Fig. 9. (a) STEM-BF image of HP 610, (b) a selected area diffraction pattern of B-phase, and (c) (d) (e) EDS mapping of HP 610.

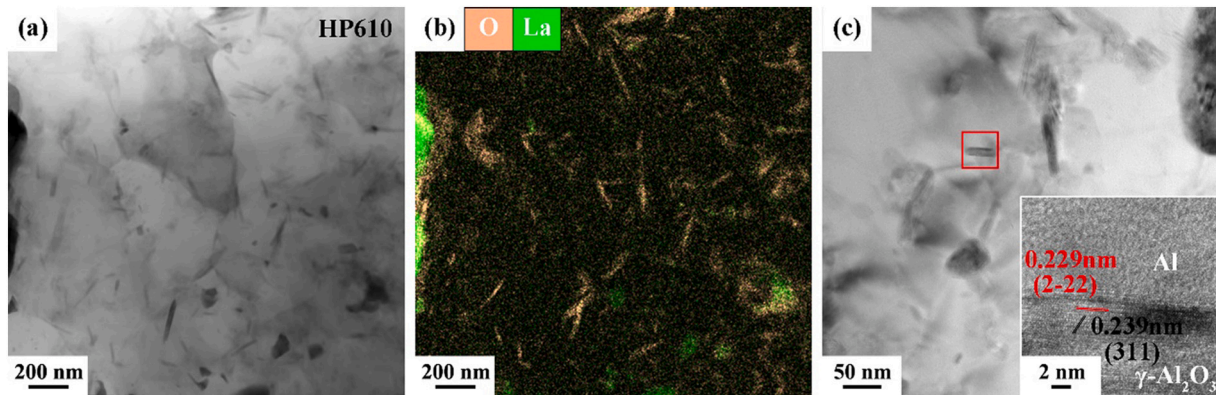


Fig. 10. (a) STEM-BF image of HP 610, (b) corresponding EDS result, and (c) TEM image of γ - Al_2O_3 with its HRTEM in the inset.

sized particles in HP 550. However, micro-sized $\text{Al}_{11}\text{La}_3$ could not be observed. AMCs fabricated by powder metallurgy with an ultrafine grain structure usually exhibited fracture surfaces with the evident character of grain boundary gliding at high temperatures [6,31,32], however, no such characteristic was disclosed in Fig. 13c and d, indicating that intergranular sliding was suppressed by the fine particles.

4. Discussion

4.1. In-situ reaction process

There are many Al–La intermetallic compounds, such as Al_4La , $\text{Al}_{11}\text{La}_3$, Al_3La , Al_2La , AlLa , and AlLa_3 , among which Al_3La and $\text{Al}_{11}\text{La}_3$ have the strongest Al–La binding force based on Debye temperature calculation [33]. According to the binary phase diagram of Al–La alloy, $\text{Al}_{11}\text{La}_3$ would be the reaction product in the investigated temperature and La content range in this study [34,35], which agreed well with the experiment result. Therefore, it could be deduced that the reaction of the Al and La_2O_3 in this study happened as follows:



In Sakamoto et al.'s study [27], the Al– La_2O_3 reaction happened during the hot-pressing process, producing γ - Al_2O_3 and $\text{Al}_{11}\text{La}_3$. However, in this study, it was found that with higher energy input, the Al– La_2O_3 reaction could happen in the HEBM process. Therefore, the in-situ reaction between Al and La_2O_3 could be divided into three processes:

4.1.1. HEBM process

In the HEBM process, am- Al_2O_3 and fine $\text{Al}_{11}\text{La}_3$ particles were produced under the severe mechanical effects. In addition to being distributed in the matrix, am- Al_2O_3 also wrapped around La_2O_3 and $\text{Al}_{11}\text{La}_3$ phases.

4.1.2. Hot-pressing process below the transformation temperature of am- Al_2O_3

At temperatures below 590 °C, am- Al_2O_3 remained in the amorphous state, still applying a shielding effect. As a result, the in-situ reaction and the coarsening of $\text{Al}_{11}\text{La}_3$ particles were slow.

4.1.3. Hot-pressing process above the transformation temperature of am- Al_2O_3

When the hot-pressing temperature reached the crystallization temperature of am- Al_2O_3 (590 °C), am- Al_2O_3 started to transform into acicular γ - Al_2O_3 . Due to the increase of hot-pressing temperature and vanishment of the barrier effect of the am- Al_2O_3 film, atom diffusion velocity was accelerated and much larger $\text{Al}_{11}\text{La}_3$ particles (about 1–2 μm in diameter) were formed.

4.2. Mechanical properties

The tensile strength of the composites at room temperature decreased with the increase of hot-pressing temperature, and the downward trend slowed significantly when the hot-pressing temperature was over 570 °C, i.e., the temperature over which the in-situ

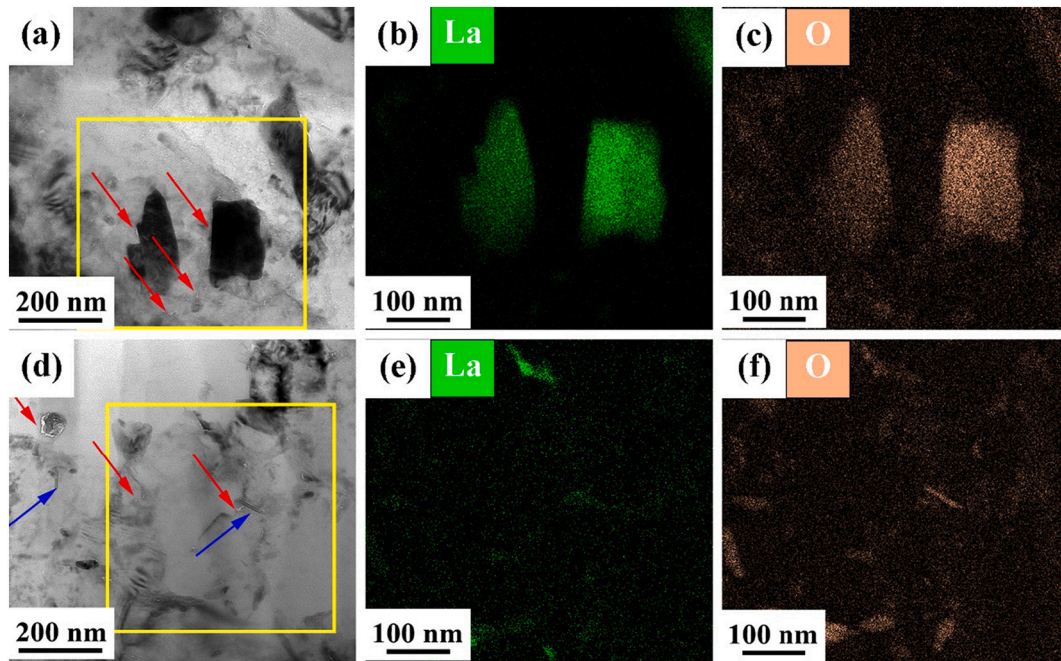


Fig. 11. (a) TEM image of HP 570, with corresponding EDS results of position denoted by yellow square being shown in (b) and (c), and (d) TEM image of HP 590, with corresponding EDS results of position denoted by yellow square being shown in (e) and (f). (For interpretation of the references to colour in this figure legend, the reader is referred to the web version of this article.)

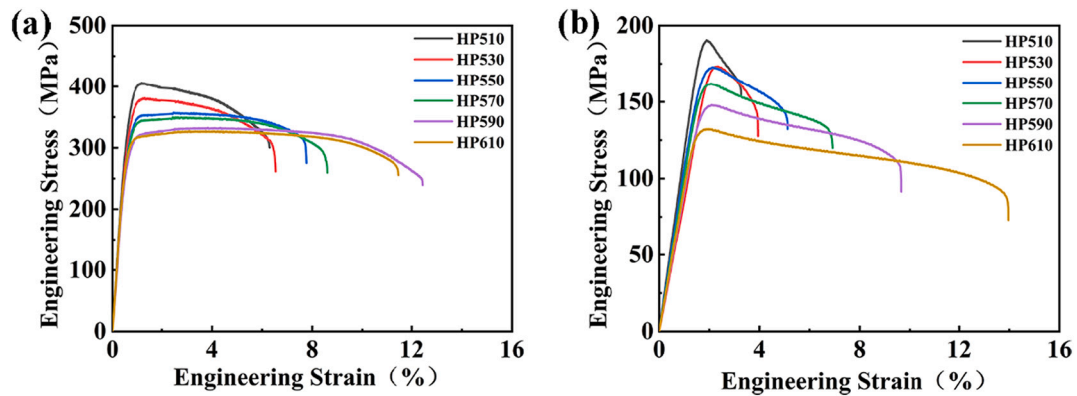


Fig. 12. Tensile stress-strain curves of the composites at (a) RT and (b) 350 °C.

Table 2
Tensile properties of the composites.

Sample	RT			350 °C		
	YS (MPa)	UTS (MPa)	EL (%)	YS (MPa)	UTS (MPa)	EL (%)
HP 510	370 ± 2	406 ± 3	6.4 ± 0.7	189 ± 6	190 ± 1	2.0 ± 0.5
HP 530	348 ± 1	381 ± 10	6.2 ± 0.1	172 ± 3	173 ± 2	2.3 ± 0.5
HP 550	328 ± 4	357 ± 9	7.2 ± 0.7	167 ± 3	173 ± 9	3.8 ± 0.8
HP 570	301 ± 4	350 ± 1	9.4 ± 1.1	159 ± 1	162 ± 1	5.5 ± 0.3
HP 590	282 ± 1	333 ± 4	12.6 ± 0.6	144 ± 3	148 ± 2	8.5 ± 0.2
HP 610	289 ± 2	327 ± 1	11.2 ± 0.1	129 ± 8	132 ± 7	12.8 ± 1.0

reaction became more sufficient, and more $\text{Al}_{11}\text{La}_3$ and $\gamma\text{-Al}_2\text{O}_3$ particles were generated.

At room temperature, the strength of AMCs is commonly enhanced by three strengthening mechanisms: (1) the load-transfer effect of micro-sized particles; (2) the grain refinement effect of nano-sized particles; and (3) the strengthening of nano-sized particles by dislocation accumulation [28].

It is known that fine particles exhibited much higher strengthening efficiency than coarse ones. When the hot-pressing temperature was lower than the crystallization temperature of am- Al_2O_3 , the in-situ reaction proceeded slowly, and the $\text{Al}_{11}\text{La}_3$ grew up with the increase of hot-pressing temperature. At the same time, higher hot-pressing temperatures resulted in coarser grains. Consequently, tensile strength decreased with the increase of hot-pressing temperature. When the hot-pressing temperature reached the crystallization temperature, Al and La_2O_3 reacted more sufficiently, resulting in a large amount of $\text{Al}_{11}\text{La}_3$ and $\gamma\text{-Al}_2\text{O}_3$, which compensated the strength loss caused by the particle coarsening. As a result, the downtrend of tensile strength slowed down when the hot-pressing temperature was over 570 °C.

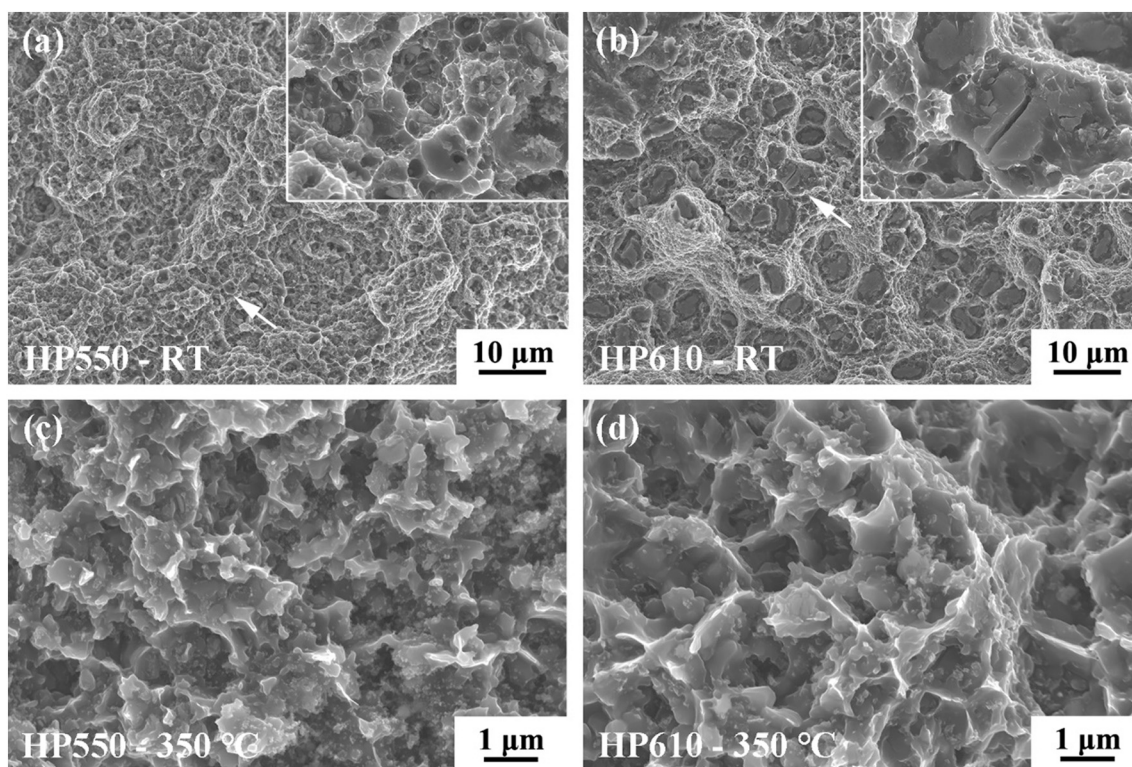


Fig. 13. SEM fractographs of HP 550 at (a) RT and (c) 350 °C, and HP 610 at (b) RT and (d) 350 °C.

At elevated temperatures, the grain boundaries were more active in sliding, migration, and grain rotation, thereby losing their strengthening effects. Also, the load-transfer effect of micro-sized particles was restricted by the relaxation process of dislocations and stress field caused by diffusional assisted flow [28]. Therefore, nano-sized particles were much more important for strengthening high-temperature strength by pinning grain boundaries and dislocations.

When the hot-pressing temperature increased, the nano-sized $\text{Al}_{11}\text{La}_3$ coarsened into a micrometer scale, losing its enhancing effect on high-temperature strength. On the other hand, the transformation of am- Al_2O_3 into $\gamma\text{-Al}_2\text{O}_3$ was reported to weaken its strengthening effect seriously [30]. As a result, the high-temperature strength of the composites decreased with the increase of hot-pressing temperature. Although a large amount of $\text{Al}_{11}\text{La}_3$ and $\gamma\text{-Al}_2\text{O}_3$ were generated at high temperatures, the high-temperature strengthening efficiency of these particles was much lower than that of nano-sized $\text{Al}_{11}\text{La}_3$ and am- Al_2O_3 , and the strength loss could not be compensated. Therefore, the high-temperature strength still decreased rapidly despite the increasing amount of $\text{Al}_{11}\text{La}_3$ and $\gamma\text{-Al}_2\text{O}_3$.

To sum up, nano-sized fine particles of am- Al_2O_3 and $\text{Al}_{11}\text{La}_3$ produced in the HEBM process exhibited much higher strengthening efficiency than $\gamma\text{-Al}_2\text{O}_3$ and micro-sized $\text{Al}_{11}\text{La}_3$ particles produced in the hot-pressing process. Tensile strength could be increased by up to 24% and 44% at room temperature and 350 °C, respectively, via maintaining Al_2O_3 in an amorphous state and $\text{Al}_{11}\text{La}_3$ in fine size.

5. Conclusions

Composites were fabricated using Al powders and La_2O_3 nanoparticles by HEBM and hot-pressing. The microstructure and mechanical properties of composites hot-pressed at different temperatures were investigated. The main conclusions are as follows.

1. The in-situ reaction was activated by HEBM, generating fine nano-sized $\text{Al}_{11}\text{La}_3$ and am- Al_2O_3 . The am- Al_2O_3 film was found to wrap

La_2O_3 and $\text{Al}_{11}\text{La}_3$, which could inhibit the reaction and coarsening of the nanoparticles.

2. At low hot-pressing temperatures (lower than 590 °C), the fine $\text{Al}_{11}\text{La}_3$ particles coarsened slowly. When the hot-pressing temperature reached 590 °C, am- Al_2O_3 film transformed into $\gamma\text{-Al}_2\text{O}_3$ particles, and reaction became more sufficient, resulting in coarse $\text{Al}_{11}\text{La}_3$ with micrometer scale.
3. Fine $\text{Al}_{11}\text{La}_3$ and am- Al_2O_3 could effectively enhance the strength of the composites. The strengthening efficiency of these particles decreased with the crystallization of Al_2O_3 and coarsening of $\text{Al}_{11}\text{La}_3$ caused by higher temperatures.
4. By controlling hot-pressing temperature, tensile strength could be increased by up to 24% and 44% at room temperature and 350 °C, respectively. The highest tensile strength at 350 °C of 190 MPa was obtained when the hot-pressing temperature was 510 °C.

Data availability

The datasets generated and/or analyzed during the current study are available from the corresponding author on reasonable request.

Declaration of Competing Interest

The authors declare that they have no known competing financial interests or personal relationships that could have appeared to influence the work reported in this paper.

Acknowledgments

The authors gratefully acknowledge the support of (a) the National Natural Science Foundation of China under grant No. 52171056, (b) CNC Science Fund for Talented Young Scholars, (c) the IMR Innovation Fund (2021-ZD02), and (d) LiaoNing Revitalization Talents Program under grant No. XLYC1902058.

References

- [1] J.C. Williams, E.A. Starke, Progress in structural materials for aerospace systems, *Acta Mater.* 51 (19) (2003) 5775–5799.
- [2] J. Abenojar, F. Velasco, M.A. Martínez, Optimization of processing parameters for the Al+10% B₄C system obtained by mechanical alloying, *J. Mater. Process. Technol.* 184 (1–3) (2007) 441–446.
- [3] N.A. Belov, D.G. Eskin, N.N. Avxentieva, Constituent phase diagrams of the Al–Cu–Fe–Mg–Ni–Si system and their application to the analysis of aluminium piston alloys, *Acta Mater.* 53 (17) (2005) 4709–4722.
- [4] Y. Nagaishi, M. Yamasaki, Y. Kawamura, Effect of process atmosphere on the mechanical properties of rapidly solidified powder metallurgy Al–Ti–Fe–Cr alloys, *Mater. Sci. Eng. A* 449–451 (2007) 794–798.
- [5] K. Hu, Q. Xu, X. Ma, Q. Sun, T. Gao, X. Liu, A novel heat-resistant Al–Si–Cu–Ni–Mg base material synergistically strengthened by Ni-rich intermetallics and nano-AlN_p microskeletons, *J. Mater. Sci. Technol.* 35 (3) (2019) 306–312.
- [6] Y.N. Zan, Y.T. Zhou, Z.Y. Liu, Q.Z. Wang, W.G. Wang, D. Wang, B.L. Xiao, Z.Y. Ma, Microstructure and mechanical properties of (B₄C+Al₂O₃)/Al composites designed for neutron absorbing materials with both structural and functional usages, *Mater. Sci. Eng. A* 773 (2020) 138840.
- [7] G. Li, H. Liao, X. Suo, Y. Tang, U.S. Dixit, P. Petrov, Cr-induced morphology change of primary Mn-rich phase in Al–Si–Cu–Mn heat resistant aluminum alloys and its contribution to high temperature strength, *Mater. Sci. Eng. A* 709 (2018) 90–96.
- [8] Y.C. Kang, S.L.I. Chan, Tensile properties of nanometric Al₂O₃ particulate-reinforced aluminum matrix composites, *Mater. Chem. Phys.* 85 (2–3) (2004) 438–443.
- [9] B. Prabhu, C. Suryanarayana, L. An, R. Vaidyanathan, Synthesis and characterization of high volume fraction Al–Al₂O₃ nanocomposite powders by high-energy milling, *Mater. Sci. Eng. A* 425 (1–2) (2006) 192–200.
- [10] K. Kallip, N.K. Babu, K.A. AlOgab, L. Kollo, X. Maeder, Y. Arroyo, M. Leparoux, Microstructure and mechanical properties of near net shaped aluminium/alumina nanocomposites fabricated by powder metallurgy, *J. Alloys Compd.* 714 (2017) 133–143.
- [11] Y. Yang, A. Kushima, W. Han, H. Xin, J. Li, Liquid-like, self-healing aluminum oxide during deformation at room temperature, *Nano Lett.* 18 (4) (2018) 2492–2497.
- [12] B. Rufino, M.V. Coulet, R. Bouchet, O. Isnard, R. Denoyel, Structural changes and thermal properties of aluminium micro- and nano-powders, *Acta Mater.* 58 (12) (2010) 4224–4232.
- [13] B. Rufino, F. Boule'h, M.V. Coulet, G. Lacroix, R. Denoyel, Influence of particles size on thermal properties of aluminium powder, *Acta Mater.* 55 (8) (2007) 2815–2827.
- [14] X. Rong, D. Zhao, C. He, C. Shi, E. Liu, N. Zhao, Revealing the strengthening and toughening mechanisms of Al–CuO composite fabricated via in-situ solid-state reaction, *Acta Mater.* 204 (2021) 116524.
- [15] H. Zhu, J. Min, J. Li, Y. Ai, L. Ge, H. Wang, In situ fabrication of (α-Al₂O₃+Al₃Zr)/Al composites in an Al–ZrO₂ system, *Compos. Sci. Technol.* 70 (15) (2010) 2183–2189.
- [16] C.F. Feng, L. Froyen, Formation of Al₃Ti and Al₂O₃ from an Al–TiO₂ system for preparing in-situ aluminium matrix composites, *Compos. A: Appl. Sci. Manuf.* 31 (4) (2000) 385–390.
- [17] M. Balog, P. Krizik, M. Nosko, Z. Hajovska, M. Victoria Castro Riglos, W. Rajner, D.-S. Liu, F. Simancik, Forged HITEMAL: Al-based MMCs strengthened with nanometric thick Al₂O₃ skeleton, *Mater. Sci. Eng. A* 613 (2014) 82–90.
- [18] S.L. Zhang, J. Yang, B.R. Zhang, Y.T. Zhao, G. Chen, X.X. Shi, Z.P. Liang, A novel fabrication technology of in situ TiB₂/6063Al composites: high energy ball milling and melt in situ reaction, *J. Alloys Compd.* 639 (2015) 215–223.
- [19] T.G. Durai, K. Das, S. Das, Al (Zn)–4Cu/Al₂O₃ in-situ metal matrix composite synthesized by displacement reactions, *J. Alloys Compd.* 457 (1–2) (2008) 435–439.
- [20] K. Wiecek-Ciurawa, D. Oleszak, K. Gamrat, Mechanosynthesis and process characterization of some nanostructured intermetallics–ceramics composites, *J. Alloys Compd.* 434–435 (2007) 501–504.
- [21] A. Heidarpour, N. Shahin, S. Kazemi, A novel approach to in situ synthesis of WC–Al₂O₃ composite by high energy reactive milling, *Int. J. Refract. Met. Hard Mater.* 64 (2017) 1–6.
- [22] W. Wan, J. Han, W. Li, J. Wang, Study of rare earth element effect on microstructures and mechanical properties of an Al–Cu–Mg–Si cast alloy, *Rare Metals* 25 (6) (2006) 129–132.
- [23] T.G. Wang, Q.C. Liang, Q. Qin, Effects of rare earth oxide La₂O₃ on microstructure and properties of Al₂O₃/Al composites, *Mater. Res. Innov.* 19 (sup5) (2015). S5–891–S5–893.
- [24] V.K. Sharma, V. Kumar, R.S. Joshi, Investigation of rare earth particulate on tribological and mechanical properties of Al-6061 alloy composites for aerospace application, *J. Mater. Res. Technol.* 8 (4) (2019) 3504–3516.
- [25] S.P. Wen, Z.B. Xing, H. Huang, B.L. Li, W. Wang, Z.R. Nie, The effect of erbium on the microstructure and mechanical properties of Al–Mg–Mn–Zr alloy, *Mater. Sci. Eng. A* 516 (1–2) (2009) 42–49.
- [26] D.H. Xiao, J.N. Wang, D.Y. Ding, H.L. Yang, Effect of rare earth Ce addition on the microstructure and mechanical properties of an Al–Cu–Mg–Ag alloy, *J. Alloys Compd.* 352 (1–2) (2003) 84–88.
- [27] T. Sakamoto, S. Kukeya, H. Ohfuji, Microstructure and room and high temperature mechanical properties of ultrafine structured Al-5 wt%Y₂O₃ and Al-5 wt%La₂O₃ nanocomposites fabricated by mechanical alloying and hot pressing, *Mater. Sci. Eng. A* 748 (2019) 428–433.
- [28] M. Balog, T. Hu, P. Krizik, M.V. Castro Riglos, B.D. Saller, H. Yang, J. M. Schoenung, E.J. Lavernia, On the thermal stability of ultrafine-grained Al stabilized by in-situ amorphous Al₂O₃ network, *Mater. Sci. Eng. A* 648 (2015) 61–71.
- [29] Y.N. Zan, Q. Zhang, Y.T. Zhou, Z.Y. Liu, Q.Z. Wang, D. Wang, B.L. Xiao, W.C. Ren, Z.Y. Ma, Introducing graphene (reduced graphene oxide) into Al matrix composites for enhanced high-temperature strength, *Compos. Part B* 195 (2020) 108095.
- [30] Z. Cvijović, M. Vratnica, I. Cvijović-Alagić, The influences of multiscale-sized second-phase particles on fracture behaviour of overaged 7000 alloys, *Proc. Eng.* 1 (1) (2009) 35–38.
- [31] Y.N. Zan, Y.T. Zhou, X.N. Li, G.N. Ma, Z.Y. Liu, Q.Z. Wang, D. Wang, B.L. Xiao, Z. Y. Ma, Enhancing high-temperature strength and thermal stability of Al₂O₃/Al composites by high-temperature pre-treatment of ultrafine Al powders, *Acta Metal. Sin. (English Letters)* 33 (7) (2020) 913–921.
- [32] G. Fan, H. Huang, Z. Tan, D. Xiong, Q. Guo, M. Naito, Z. Li, D. Zhang, Grain refinement and superplastic behavior of carbon nanotube reinforced aluminum alloy composite processed by cold rolling, *Mater. Sci. Eng. A* 708 (2017) 537–543.
- [33] F. Sun, G. Zhang, X. Ren, M. Wang, H. Xu, Y. Fu, Y. Tang, D. Li, First-principles studies on phase stability, anisotropic elastic and electronic properties of Al–La binary system intermetallic compounds, *Mater. Today Commun.* 24 (2020) 101101.
- [34] S.H. Zhou, R.E. Napolitano, Phase equilibria and thermodynamic limits for partitionless crystallization in the Al–La binary system, *Acta Mater.* 54 (3) (2006) 831–840.
- [35] J. Wang, Thermodynamic optimization for al-la system, *Calphad* 18 (3) (1994) 269–272.